Stability Analysis of the Slowed-Rotor Compound Helicopter Configuration

Matthew W. Floros
US Army Research Laboratory
Hampton, Virginia

Wayne Johnson
Army/NASA Rotorcraft Division
NASA Ames Research Center
Moffett Field, California

The stability and control of rotors at high advance ratio are considered. Teetering, articulated, gimbaled, and rigid hub types are considered for a compound helicopter (rotor and fixed wing). Stability predictions obtained using an analytical rigid flapping blade analysis, a rigid blade CAMRAD II model, and an elastic blade CAMRAD II model are compared. For the flapping blade analysis, the teetering rotor is the most stable, showing no instabilities up to an advance ratio of 3 and a Lock number of 18. A notional elastic blade model of a teetering rotor is unstable at an advance ratio of 1.5, independent of pitch frequency. Analysis of the trim controls and blade flapping shows that for small positive collective pitch, trim can be maintained without excessive control input or flapping angles.

Nomenclature

k_p	blade pitch-flap coupling ratio
β	rigid blade flap angle
γ	Lock number
δ_3	blade pitch-flap coupling angle
ν_β	fundamental flapping frequency
ω	dominant blade flapping frequency
μ	rotor advance ratio
ν_θ	blade fundamental torsion frequency
$\dot{(\ )}$	derivative with respect to azimuth

Introduction

Recently there has been increased interest in expanding the flight envelope of rotorcraft, particularly in terms of speed, altitude, and range. Increased range allows attack, scout, and rescue aircraft to reach farther from their bases. Additional speed and altitude capability increases the survivability of military vehicles and cost efficiency of civilian aircraft. Long loiter times improve the effectiveness of scout aircraft, with particular applications of interest being unmanned aerial vehicles (UAVs) and homeland security surveillance aircraft.

Much work has been focused on tilt rotor aircraft; both military and civilian tilt rotors are currently in development. But other configurations may provide comparable benefits to tilt rotors in terms of range and speed. Two such configurations are the compound helicopter and the autogyro. These configurations provide short takeoff or vertical takeoff capability, but are capable of higher speeds than a conventional helicopter because the rotor does not provide the propulsive force. At high speed, rotors on compound helicopters and autogyros with wings do not need to provide the vehicle lift. The drawback is that redundant lift and/or propulsion systems add weight and drag which must be compensated for in some other way.

One of the first compound helicopters was the McDonnell XV-1 "Convertiplane," built and tested in the early 1950s. There are many novel design features in this remarkable aircraft (Refs. 1–4), which was tested in the NACA 40- by 80-Foot Wind Tunnel at the Ames Aeronautical Laboratory (Ref. 5) and flight tested near McDonnell's St. Louis, Missouri facilities (Ref. 6). The aircraft successfully flew in its three distinct operating modes, helicopter, autogyro, and airplane, and could transition smoothly between them.

One of the features of the XV-1 was that in airplane mode, the rotor would be slowed to a significantly lower speed to reduce its drag in forward flight. The combination of high forward speed and low rotor speed produced an advance ratio near unity, which is far above what is typical for conventional edgewise rotors.

Other prototype compound helicopters since the XV-1 include the Fairey Rotodyne and the Lockheed Cheyenne. Prototypes of both aircraft were built and flown, but never entered production. Recently, CarterCopters and Groen Brothers have developed autogyro demonstrators and have proposed autogyros and compound helicopters for future heavy lift and unmanned roles.

Previously, the performance of slowed-rotor compound

Presented at the American Helicopter Society 60th Annual Forum, Baltimore, MD, June 7–10, 2004.

aircraft was examined with isolated rotor and rotor plus fixed wing analytical models (Ref. 7). The purpose of the current effort is to examine the stability of slowed-rotor compound aircraft, particularly at high advance ratios.

In the present study, rigid blade flapping stability is examined with a simplified analysis and with the comprehensive analysis CAMRAD II. Elastic blade stability is also calculated with CAMRAD II. Finally, performance and trim are examined for teetering and articulated rotors.

Flap Stability

The simplified analysis predictions are based on rigid flapping blade equations similar to those developed by Sissingh (Ref. 8). These equations were used by Peters and Hohenemser (Ref. 9) to examine flapping stability of an isolated blade and a four-bladed gimbaled rotor with tilt-moment feedback. In the present study, they are used to compare different hub configurations in order to assess suitability for high advance ratio operation.

The analysis addresses only rigid blade flapping; lag and torsion motion are not modeled. The aerodynamics are linear and aerodynamic coefficients are obtained by integrating analytically along the blade length. The flapping blade equations are integrated over a single rotor revolution and Floquet theory is used to determine the system stability. The homogeneous flapping blade equation is given by

$$\ddot{\beta} - \gamma M_{\dot{\beta}} \dot{\beta} + (\nu_\beta^2 - \gamma M_\beta + \gamma k_p M_\theta)\beta = 0 \qquad (1)$$

In this expression, $M_{\dot{\beta}}$, M_β, and M_θ are the aerodynamic coefficients. The blade motion is thus defined by only the flap frequency, Lock number, advance ratio (embedded in the aerodynamic coefficients) and pitch-flap coupling. The pitch-flap coupling ratio and the more commonly used δ_3 angle are related by $k_p = \tan\delta_3$.

For the present study, multi-blade equations were derived for articulated and gimbaled (three bladed) rotors, as well as teetering and an XV-1-type gimbaled rotor. The latter two configurations were not addressed in Ref. 9. The teetering and gimbaled rotors are straightforward. The teetering rotor has only a single degree of freedom for the teeter motion; coning is not allowed. For the gimbaled rotor, there are two cyclic degrees of freedom and a coning degree of freedom.

The XV-1 rotor is more complicated. It has a three-bladed gimbaled rotor with offset coning hinges. The gimbal motion has a flap frequency of $\nu_\beta = 1$/rev and pitch-flap coupling angle $\delta_3 = 15$ deg. The coning motion has a flap frequency of $\nu_\beta = 1.1$/rev and $\delta_3 = 65.6$ deg. To model the XV-1 rotor in the context of the simplified analysis, the appropriate constants were used in each of the multi-blade equations. For the two cyclic equations, $\nu_\beta = 1$/rev and $\delta_3 = 15$ deg were used, and for the coning equation, $\nu_\beta = 1.1$/rev and $\delta_3 = 65.6$ deg were used.

A series of stability maps for an articulated rotor with flap frequency $\nu_\beta = 1$/rev is shown in Fig. 1. In each plot, the damping contours are shown as solid lines, positive numbers indicating positive damping, and negative numbers indicating an instability. Only the damping of the least stable root is shown. The dashed lines separate regions where the dominant frequency of the root is $1 \pm n$/rev, $0.5 \pm n$/rev, or non-harmonic frequencies. Dominant system frequencies of 1/rev and 0.5/rev occur when the Floquet roots are on the real axis, whereas the frequency is non-harmonic when the roots are complex conjugates.

Specific frequencies are identified by solving the flapping equation in hover, where the coefficients are constant rather than periodic. The roots of the system are given by

$$s = -\frac{\gamma}{16} \pm i\sqrt{\nu_\beta^2 + \frac{\gamma}{8}k_p - \left(\frac{\gamma}{16}\right)^2} \qquad (2)$$

The frequency, ω, is the imaginary part, and can be solved for γ as

$$\gamma = 16\left(k_p \pm \sqrt{k_p^2 + \nu_\beta^2 - \omega^2}\right) \qquad (3)$$

The hover Lock numbers for a blade frequency ν_β of 1.0 are given in Table 1. Missing Lock numbers indicate that the roots are complex numbers.

The pitch-flap coupling varies from 0 to 65.6 deg in the four plots. The 65.6 deg angle was chosen because the coning hinges on the XV-1 have 65.6 deg of δ_3. Increasing δ_3 (Figs. 1a-c) increases the flapping stability margin such that at δ_3 of 30 deg, there is no unstable region in this range of advance ratio and Lock number. Once δ_3 exceeds about 45 deg, the damping at high advance ratio declines again. Fig. 1d shows δ_3 of 65.6 deg and includes several unstable regions with the stability boundary occurring at a lower advance ratio than $\delta_3 = 0$ (Fig. 1a). The plots suggest that an articulated blade can be used at advance ratios higher than 2 if appropriate δ_3 is included.

Stability maps for a teetering rotor are shown in Fig. 2. The teetering rotor stability is quite different from that of the articulated blade. The stability is much less dependent on advance ratio throughout the entire δ_3 and Lock number range. The effect of δ_3 on damping is also much less pronounced than in the single blade case. The damping magnitudes change with changes in δ_3, but the characteristic shape remains the same. The damping is level or slightly increasing up to an advance ratio of unity, then gradually decreases at higher advance ratios. This simple analysis suggests that a teetering rotor is a good candidate for a high advance ratio rotor.

Results for a rigid gimbaled rotor are shown in Fig. 3. For these results, a 3-bladed rotor with only the gimbal motion

Table 1. Hover Lock numbers for a rotor with flap frequency $\nu_\beta = 1.0$

k_p	δ_3	$\omega = 0$	$\omega = 0.5$	$\omega = 1.0$	$\omega = 1.5$	$\omega = 2.0$	$\omega = 2.5$
0	0	16	13.9	0	–	–	–
0.268	15	20.9	18.8	8.6	–	–	–
0.577	30	27.7	25.9	18.5	–	–	–
2.2	65.6	74.0	73.2	70.5	4.9, 65.5	13.5, 56.9	–

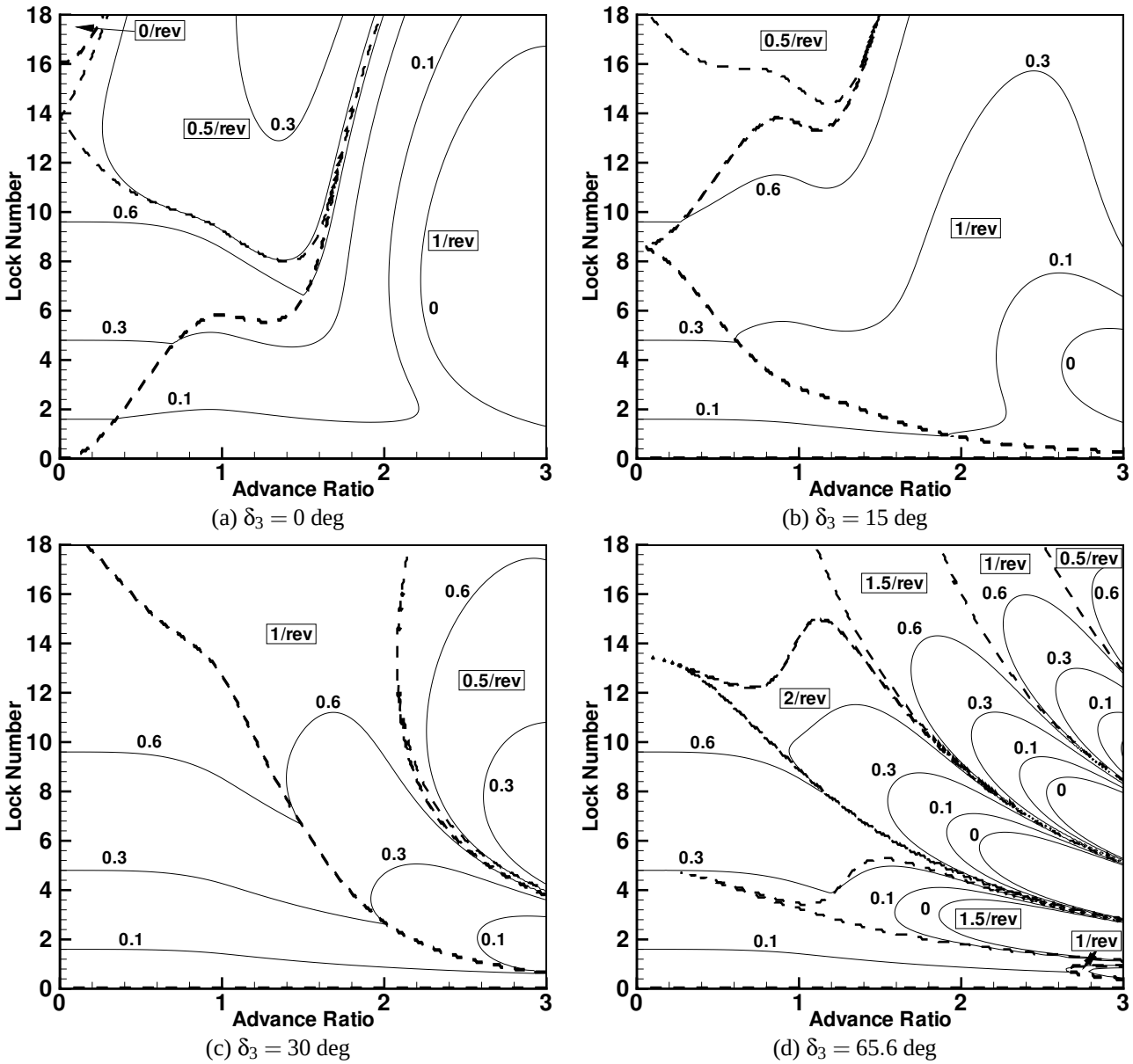

(a) $\delta_3 = 0$ deg (b) $\delta_3 = 15$ deg

(c) $\delta_3 = 30$ deg (d) $\delta_3 = 65.6$ deg

Fig. 1. Stability maps of a rigid blade articulated rotor at 0, 15, 30, and 65.6 deg of δ_3, ν_β = 1.0.

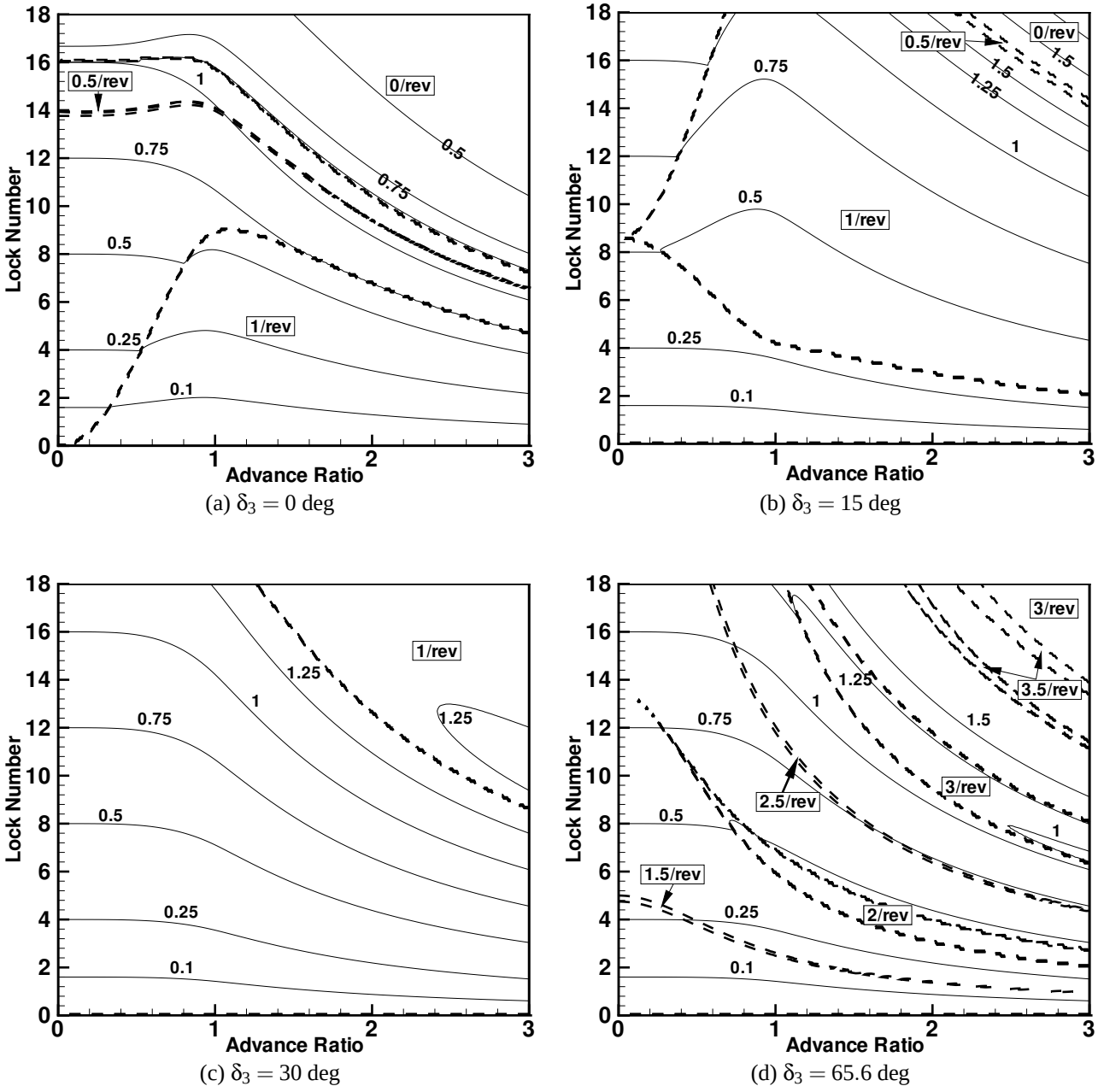

(a) $\delta_3 = 0$ deg (b) $\delta_3 = 15$ deg

(c) $\delta_3 = 30$ deg (d) $\delta_3 = 65.6$ deg

Fig. 2. Stability maps of a rigid blade teetering rotor at 0, 15, 30, and 65.6 deg of δ_3.

(specifically two cyclic modes) is considered. Like the articulated and teetering rotors, the flap frequency is $\nu_\beta = 1.0$. From these plots, an advance ratio limit near $\mu = 2$ is evident. For no pitch flap coupling, Fig. 3a, an instability occurs around $\mu = 1.5$. Increasing δ_3 to 15-30 deg delays the onset of this instability to about $\mu = 2$ (Fig. 3b-c), but additional δ_3 does not delay the onset further (Fig. 3d). This suggests that an inherent limit exists that can only be alleviated slightly with δ_3, at least without coning motion.

A production gimbaled rotor would not be rigid in coning. It would either have coning hinges, like the XV-1, or it would have a coning mode due to elastic bending of the blades. In either case, the coning mode would have a frequency greater than 1. The coning mode of a 3-bladed gimbaled rotor is shown in Fig. 4. For this plot, the coning equation which was neglected for Fig. 3 was solved separately. To match the coning mode of the XV-1, the flap frequency for these plots has been increased to $\nu_\beta = 1.1$.

For this mode, no instability is seen for any of the plots. The damping contours are relatively independent of advance ratio, and change very little with increasing δ_3. Although the frequency contours change dramatically with δ_3, the damping contours appear to change only in the vicinity of the frequency boundaries.

The stability map for the XV-1 rotor is shown in Fig. 5. If there were no coupling between the gimbal and coning modes, this plot would be the combination of Figs. 3b and 4d. There are two large instability regions, the high Lock number region with a 0.5/rev frequency, and the low Lock number region, whose frequency is not locked to 0.5/rev or 1/rev. The low Lock number region extends down to an advance ratio of about 1.4. The Lock number at this minimum point is very close to the 4.2 Lock number of the XV-1.

Ref. 3 identified a 0.5/rev instability in a test model at $\mu \approx 1.5$. Such a stability boundary agrees well with the current prediction, but the frequencies do not agree. The thin areas enclosed by the dashed lines in the lower right of Fig. 5 are frequency locked at 0.5/rev, but outside these small regions the frequency is not locked.

CAMRAD II Teetering Rotor Model Description

The flapping blade analysis provides a broad picture of the stability of a number of rotor configurations, Lock numbers, and advance ratios, but is limited in usefulness by its many simplifications. To go beyond the guidance provided by the flapping blade analysis, a slowed-rotor vehicle model based on the CarterCopter Technology Demonstrator, or CCTD (Ref. 10), was developed for the comprehensive analysis CAMRAD II (Ref. 11). The model was previously used to examine the performance (Ref. 7) of the slowed-rotor concept and in the present study is used to examine stability and control. Since little detailed information is publicly available about the prototype, the analytical model is relatively simple. It is intended only to capture the basic geometries of the rotor and wing of the aircraft as an alternative to inventing a geometry (see Fig. 6). The maximum gross weight of the demonstrator is approximately 4200 lb.

Both rigid blade and elastic blade models were developed. The models were developed to investigate parameter variations applicable to slowed-rotor vehicles in general rather than to model the CCTD design specifically in detail. The rigid blade analysis does not allow for elastic bending or torsion, so many details of the mass and stiffness distributions and aerodynamic center offsets are unnecessary. For the elastic blade analysis, the rotor was made as simple as possible to avoid introduction of additional unknowns into the results. The properties of the rotor and wing are shown in Table 2.

The CCTD prototype rotor has an extremely low Lock number caused by the presence of a 65 lb mass in each blade tip. These masses provide rotational inertia to store enough energy in the rotor for a jump take-off. For the present study, variations in chordwise offset of masses were not considered. The tip masses were placed on the quarter chord for both the rigid and elastic blade models.

For the actual aircraft, the blade and wing use NACA 65-series airfoils. Airfoil tables were not available for the airfoils on the demonstrator, so the NACA 23012 was used as a substitute. The wing model is straightforward. The wing is swept, tapered, and untwisted, with an aspect ratio of 13.4. The lifting line aerodynamic model of the wing in CAMRAD II is identical to the aerodynamic model used for the rotor blades.

Before discussing trim, some definitions should be noted. The CCTD is an autogyro, so while it is flying, there is no torque applied to the rotor shaft. The XV-1 also operated in this mode at high speed. In the context of this paper, the word *autorotation* describes the trim state of the rotor, where rotor speed is maintained with no torque input to the shaft. For a helicopter, autorotation of the rotor implies that an emergency landing is in process, but for an autogyro, the rotor is in an autorotation state for normal cruise flight. These should not be confused. *Rotor power*, when used in reference to an autorotating rotor, is defined here as the rotor drag multiplied by its velocity. This power is indirectly supplied by the aircraft's propulsion system (which overcomes the drag) and not shaft torque.

Several trim variables were used. The CCTD is controlled only with collective pitch and tilt of the spindle to which the rotor is attached. For the calculations, spindle tilt was modeled by tilting the rotor shaft. If the rotor is trimmed in autorotation, the shaft torque must be zero. The spindle tilt was used to control the shaft torque. The incidence angle of the wing was used to trim the vehicle lift. By using wing incidence and spindle tilt, the controls are largely independent of each other. Shaft angle affects both rotor lift and shaft torque, but wing incidence does not have any effect on the rotor lift or power. Cyclic pitch was not used for trim in any of the calculations.

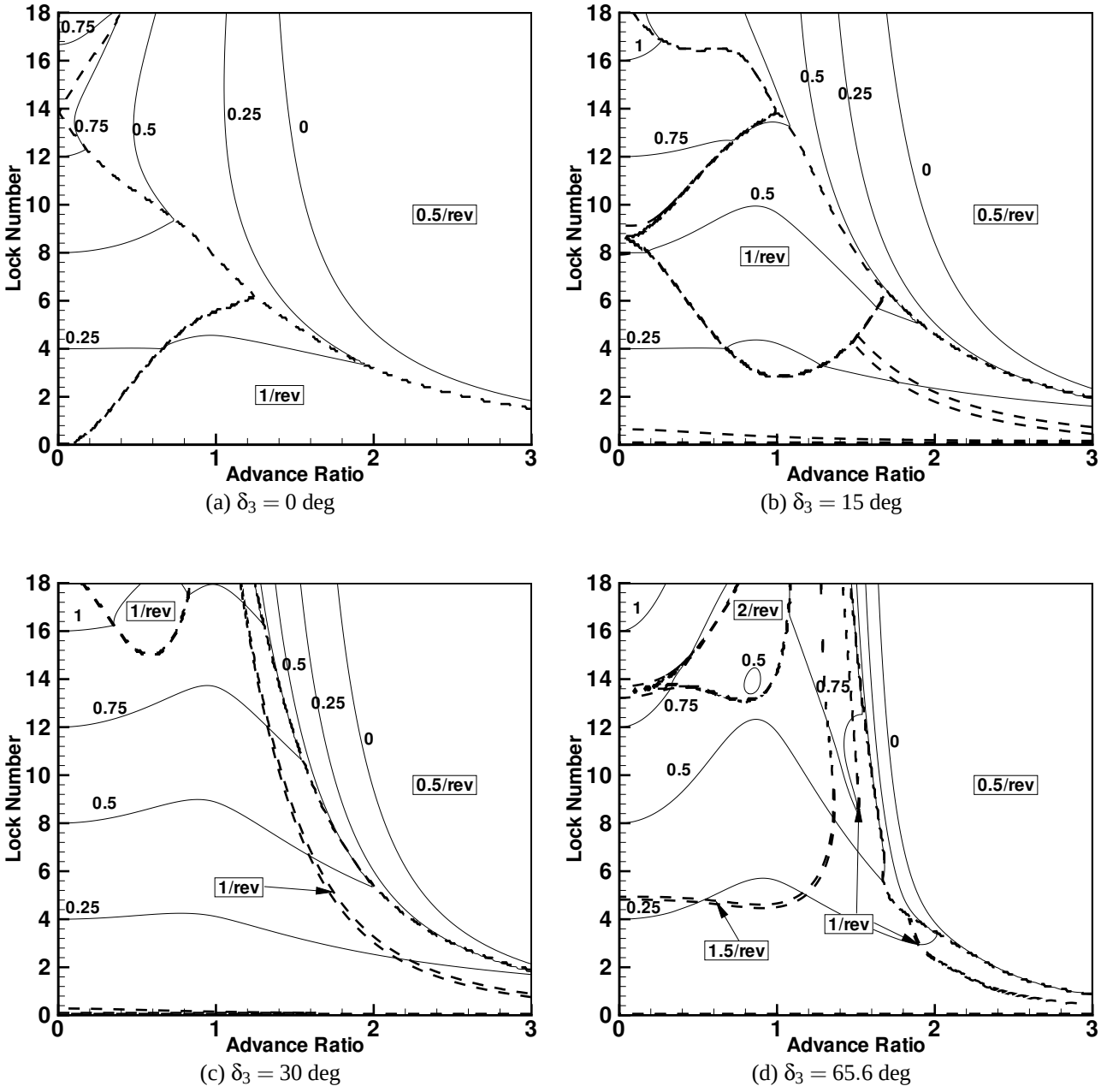

(a) $\delta_3 = 0$ deg

(b) $\delta_3 = 15$ deg

(c) $\delta_3 = 30$ deg

(d) $\delta_3 = 65.6$ deg

Fig. 3. Stability maps of cyclic modes of a rigid blade gimbaled rotor at 0, 15, 30, and 65.6 deg of δ_3.

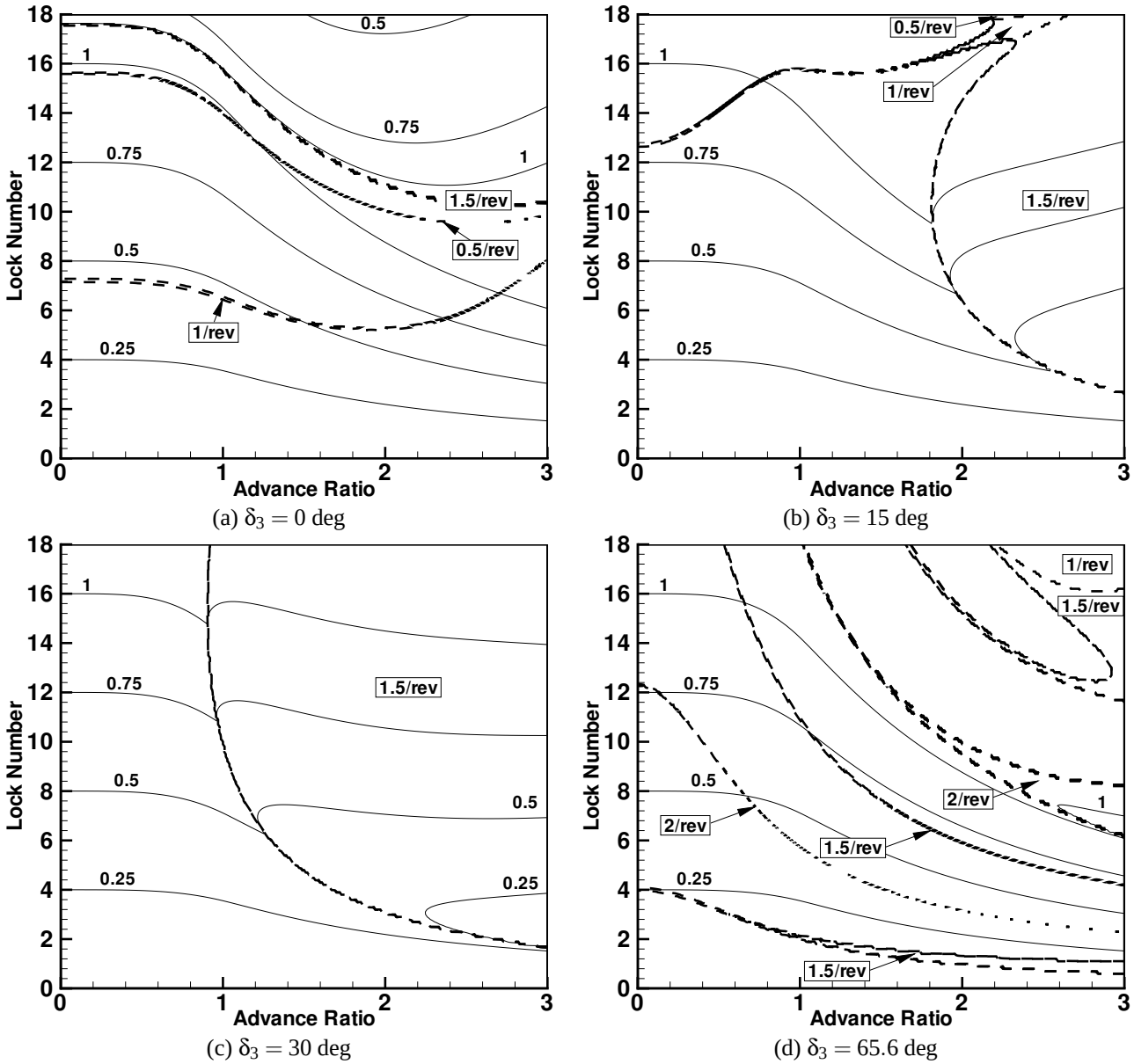

(a) $\delta_3 = 0$ deg (b) $\delta_3 = 15$ deg

(c) $\delta_3 = 30$ deg (d) $\delta_3 = 65.6$ deg

Fig. 4. Stability maps of only the coning mode of a rigid blade gimbaled rotor with coning hinge at 0.062R and 0, 15, 30, and 65.6 deg of δ_3, ν_β = 1.1.

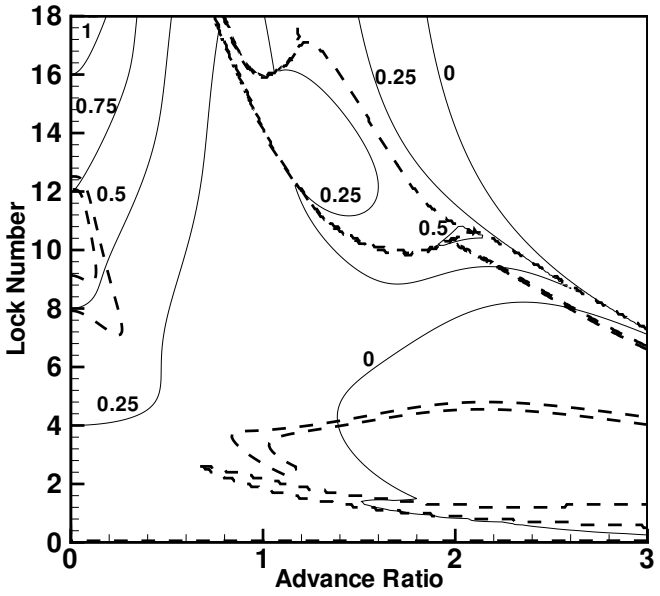

Fig. 5. Stability map for XV-1 rotor, $\delta_{3,g}$ = 15 deg $\delta_{3,c}$ = 65.6 deg, $\nu_{\beta,c}$ = 1.1, $\nu_{\beta,g}$ = 1.0.

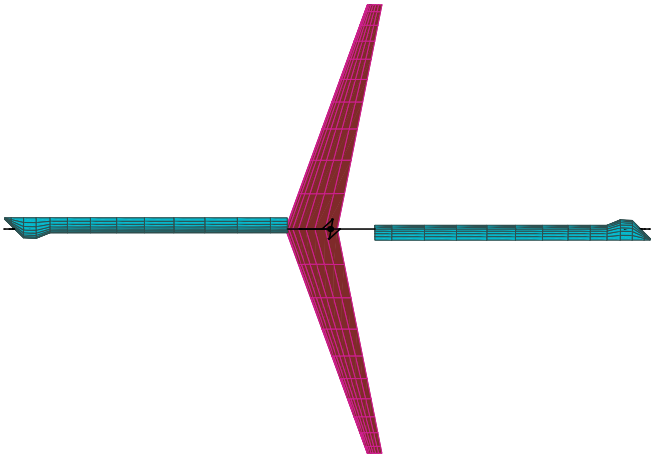

Fig. 6. Top view of CAMRAD II rotor and wing model, $\psi = 0$ deg, direction of flight to left.

An additional, implicit trim condition for a teetering rotor is that the hub moment must be zero. This condition is normally accommodated by flapping.

Ref. 7 presented correlation of CAMRAD II calculated trim and performance with wind tunnel measurements. While in that work a vortex wake model was used, it was found that the induced drag of both the rotor and wing were small. Hence a uniform inflow model (based on momentum theory) is used for the present results.

Comparison of CAMRAD II Model to Simple Analysis

The simplified analysis described above was compared with the rigid blade CAMRAD II model to determine what differences would be introduced by more sophisticated aerodynamics and blade motion, airfoil tables, etc. To model the CCTD using the simplified analysis, a δ_3 of 10 deg was selected and the Lock number and advance ratio were varied as in the previous results. The stability map for a teetering rotor with 10 deg of δ_3 is shown in Fig. 7.

Stability calculations were performed for the CAMRAD II model with the rotor trimmed and untrimmed. For the untrimmed condition, the rotor collective was fixed at 1 deg and the rotor shaft was fixed at 0 deg. The rotor could flap freely and there was no zero torque constraint on the rotor. The tip speed was selected as 230 ft/sec to minimize compressibility effects at high advance ratio. The result is shown in Fig. 8. For the majority of the plot, the damping levels are very similar to those in Fig. 7. At high Lock numbers and advance ratios above 2, the plots begin to differ, as the damping increases in the simplified analysis, but decreases in the CAMRAD II calculation.

The calculation was repeated, enforcing the autorotation condition. Here, the shaft angle was varied to maintain zero power on the rotor. This trimmed result is shown in Fig. 9. Note that the data only extends to an advance ratio of 2. It was difficult to find a stable autorotation condition at the higher Lock numbers. As the advance ratio approached 2, the analysis predicted a rapid change in trim shaft angle, suggesting that the rotor stall was preventing autorotation.

The damping contours for the trimmed case are also similar to the simplified analysis except in the high advance ratio, high Lock number region where the rotor begins to stall. This means that when the rotor is lifting, the damping is unaffected by nonlinear aerodynamics and dynamics, the introduction of a real airfoil, and trim. The simplified analysis is a good approximation for a rigid flapping blade. Note that for a 230 ft/sec tip speed, an advance ratio of 2 corresponds to nearly 275 knots, which is very high speed for a rotary-wing vehicle.

Control of Thrust and Autorotation

The performance analysis in Ref. 7 suggested that there was a narrow range of collective pitch where the rotor was autorotating at the desired speed and producing positive lift. The most desirable condition for low vehicle power is for the wing to lift the vehicle and for the rotor to produce no lift and as little drag as possible. Of course, the rotor must produce some thrust in order to maintain autorotation, so a more realistic condition is for the rotor to produce a small positive thrust. Conditions where the rotor produces negative thrust or a significant portion of the vehicle lift are undesirable.

Producing too much lift rotor lift normally requires excess power and reduces the vehicle efficiency, but does not pro-

Table 2. Properties of the model rotor and wing

Rotor	
Number of Blades	2
Hub type	teetering
Radius	22 ft
Root chord	17 in
Tip chord	7 in
Solidity	0.032
Lock number	2.3
Twist	0 deg
Airfoils	NACA 23012
δ_3	10 deg
Wing	
Span	32 ft
Root chord	45 in
Tip chord	12.5 in
Aspect ratio	13.4
Sweep angle	18 deg
Incidence angle	5.2 deg
Dihedral	6 deg
Wash out	none
Airfoil	NACA 23012
Position	(8.9, 2.63) ft below, forward of rotor

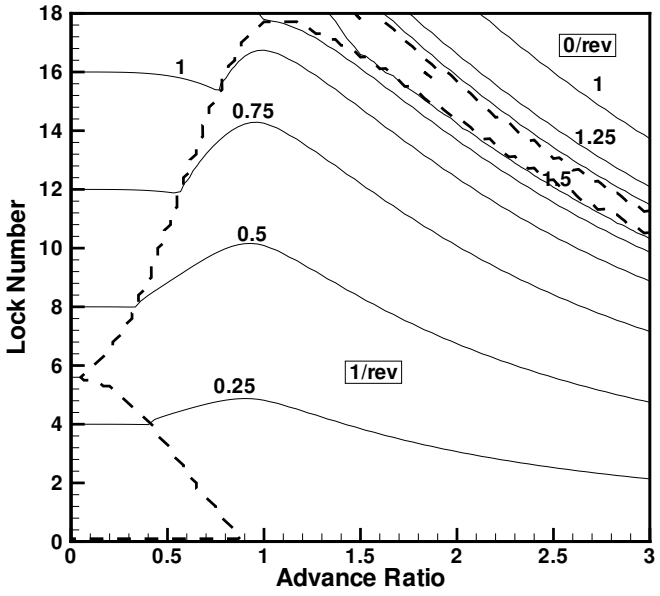

Fig. 7. Stability map for CarterCopter rotor from simplified analysis, δ_3 = 10 deg, ν_β = 1.0 ($\gamma \approx 2.5$ for CarterCopter).

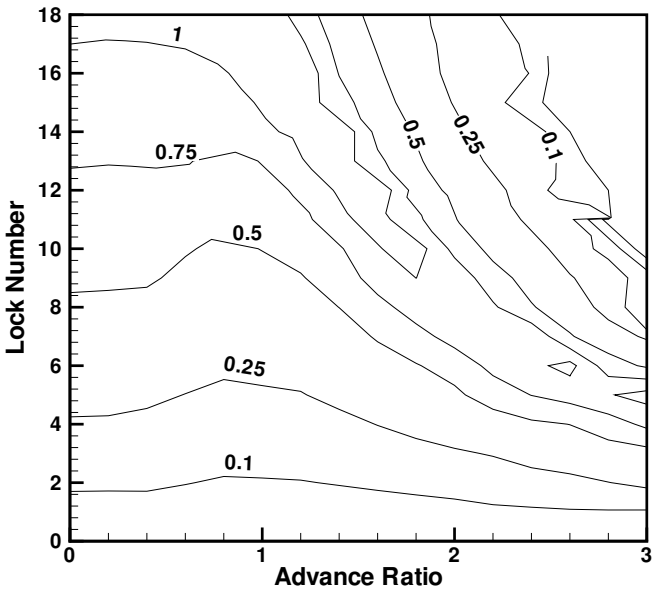

Fig. 8. Stability map for CarterCopter rotor from CAMRAD II rigid blade model, δ_3 = 10 deg, ν_β = 1.0, no trim.

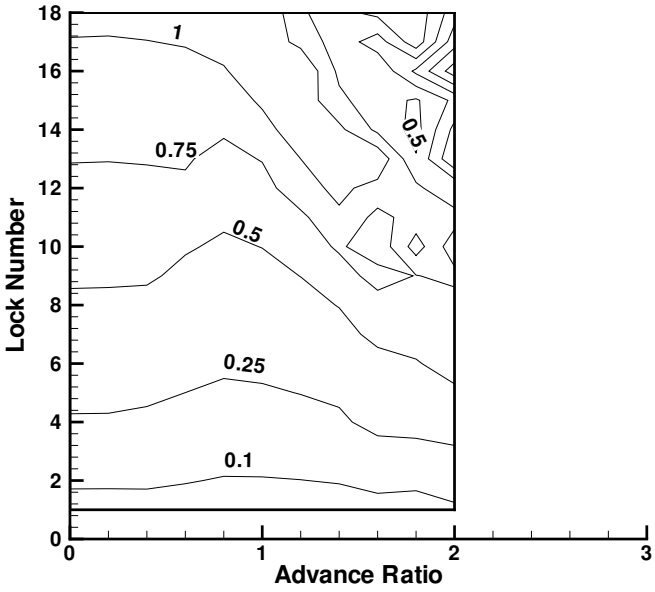

Fig. 9. Stability map for CarterCopter rotor from CAMRAD II rigid blade model, δ_3 = 10 deg, ν_β = 1.0, trimmed to autogyro condition.

hibit operation. Excessive flapping or control input requirements, however, might prevent the vehicle from operating safely. These represent flying qualities issues if they exceed the abilities of control actuators or of the pilot.

To determine the sensitivity of these variables to collective pitch and advance ratio, the rotor-wing combination described above was trimmed at tip speeds of 230, 345, and 460 ft/sec for teetering and articulated hubs. The articulated hub had no hinge offset, but results in (Ref. 12) showed that a 5% hinge offset produced nearly identical results to that with no hinge offset. Ref. 12 also presented results for a rigid rotor with no hinges or flap flexibility, but such a configuration could not be trimmed in rolland is not presented here. The rotors were identical in geometry to the model in the previous section; only the hub boundary condition was changed.

As in Ref. 7, only lift and rotor power were trimmed for these calculations. The lift of the rotor and wing combination was trimmed to 4200 lb and the rotor torque was trimmed to zero to model lifting the vehicle gross weight and an autorotation condition on the rotor. Trim controls were tilt of the wing and rotor shaft, but there was no cyclic pitch on the rotor.

Before proceeding, an interesting aspect of the autorotation envelope must be discussed. The trim state in autorotation is not unique. Two conditions exist where the rotor can maintain autorotation. To illustrate this phenomenon, isolated rotor power of an articulated rotor was considered while sweeping the shaft angle. Instead of trimming the rotor to zero power, the shaft angle was changed and the RPM held fixed. This was intended to determine if the resulting power curve crosses through zero in multiple places, indicating multiple autorotation states.

Fig. 10 shows thrust and power for an articulated rotor hinged at the root at 250 knots and a tip speed of 345 ft/sec. Collective pitch angles of -2, 0, and 2 deg are shown in the figure. The rotor power (solid lines) peaks at different shaft angles depending on the collective pitch. But for each shaft angle, the power curve crosses zero power in two places about 4 deg apart. This means that autorotation can be maintained at either of these shaft angles. In addition, the overlaid rotor thrust (dashed lines) shows that for each collective pitch setting, one trim condition has positive thrust and the other has negative thrust. Note that the thrust difference between the two points is on the order of 2000 lbs, a substantial amount for a 4200-lb vehicle.

This raises questions about whether a maneuver could cause the rotor to switch abruptly between the two autorotation points. Transient analysis of a full vehicle is beyond the scope of this paper, so this issue is not considered in detail. For the purposes of this paper, the only consequence of multiple trim conditions is that care was taken to always trim to the higher thrust condition. The large difference in thrust between the two trim states makes it easy to identify when the analysis has trimmed to the wrong thrust. Fortunately, judicious selection of initial conditions was all that was necessary to reach the desired trim condition.

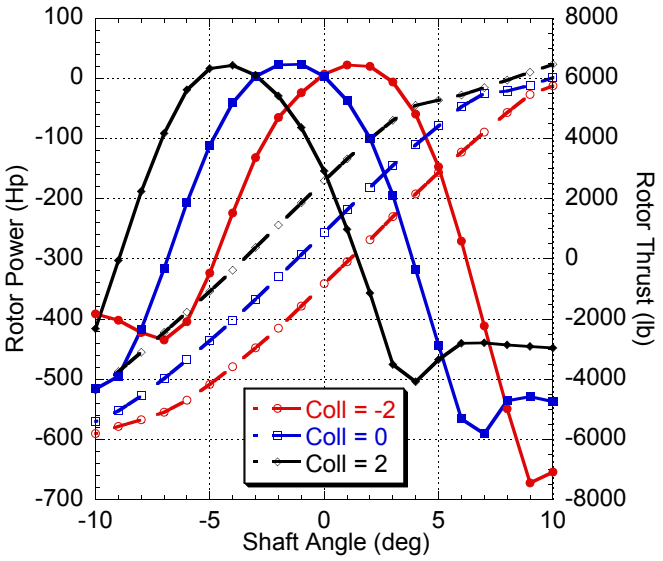

Fig. 10. Rotor thrust (open and dashed) and power (closed and solid) for an articulated rotor at 250 knots (μ = 1.22) vs. shaft angle, -2 to 2 deg collective, V_T = 345 ft/sec.

Teetering Rotor

The control issue raised in Ref. 7 was based on teetering rotor performance calculations. The lift distributions for the rotor and wing suggested that there was a narrow range of collective pitch settings where the rotor produced an acceptable thrust level. Rotor lift as a function of airspeed and collective pitch for the teetering rotor model is shown in Fig. 11. The contours indicate lines of constant lift and the dashed lines indicate negative lift. From these figures, there does seem to be a small range of acceptable collective pitch. At the lowest tip speed, Fig. 11a, there is a relatively large range of rotor lift in the 4 deg collective pitch range shown. At 250 kts, the lift changes by approximately 1500 lb over that range. At very high speed, the lift becomes negative for collective pitch settings above 0.5 deg and the range of lift is on the order of the 4200 lb gross weight of the CCTD. Below 250 kts, the desired small positive lift is realized over the entire range.

The 345 ft/sec tip speed case, shown in Fig. 11b, shows similar behavior, albeit over a larger collective pitch range. As with the lower tip speed case, the change in lift over the pitch range shown (6 deg for this tip speed) is also about 1500 lb at 250 kts and increases thereafter. Also like the lower tip speed, there does not appear to be any lift issue for airspeeds below 250 kts.

For the highest tip speed, Fig. 11c, compressibility dominates the vehicle lift above 250 kts. Operating at high airspeeds for this tip speed is not practical due to the high power

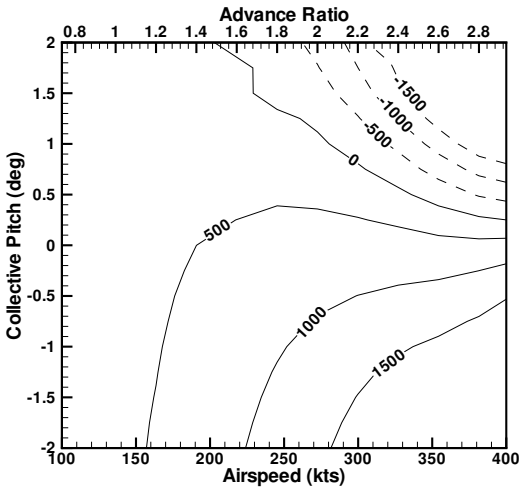

(a) V_T = 230 ft/sec

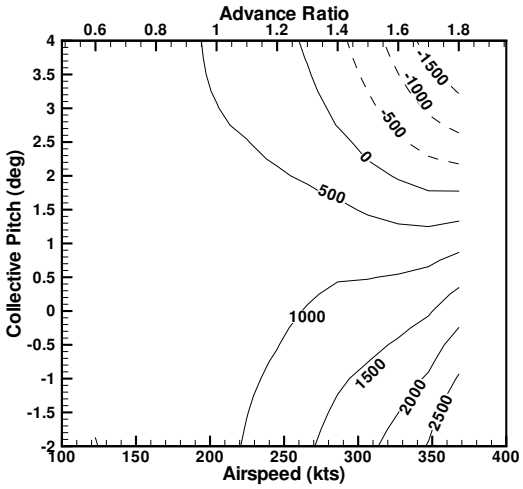

(b) V_T = 345 ft/sec

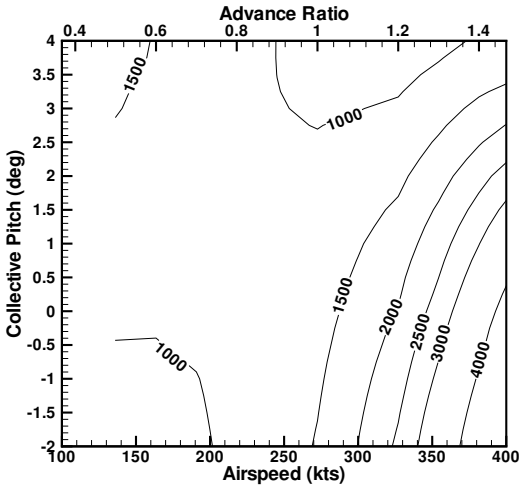

(c) V_T = 460 ft/sec

Fig. 11. Lift for a teetering rotor vs. airspeed and collective pitch, V_T = 230–460 ft/sec.

required (Ref. 7). In summary, while there is the potential for some degradation in performance when operating at a non-optimum collective, small variations will not radically alter the lift on the rotor.

Although the rotor lift was well-behaved over a range of airspeed and collective pitch, large gradients in flapping or controls indicate a handling qualities and perhaps vehicle stability problem. The spindle tilt and blade flapping angles are shown in Figs. 12 and 13. Both the spindle tilt and blade flapping are well-behaved.

The spindle tilt (positive aft) is shown in Fig. 12. It changes with airspeed at low collective pitch, but as speed increases, it is relatively independent of airspeed for all three tip speeds. The reason for this is the vehicle trim. At low speed, the wing (and therefore fuselage) must be at a high angle of attack to carry most of the vehicle weight. As speed and dynamic pressure increase, this angle decreases. For the rotor to maintain its orientation in space, the spindle must be tilted aft to account for the wing angle of attack.

The flapping angle (positive forward), shown in Fig. 13, is also well-behaved. For the 230 and 345 ft/sec tip speeds, the contours are parallel and the range of flapping is about the same as the range of collective pitch. If possible, flapping should be minimized, so for the range of collective pitch settings shown, lower collective pitch is better. For the 460 ft/sec case (Fig. 13c), although the contours are inclined at a steeper angle and the flapping range is slightly larger, there are no steep gradients and the maximum flapping angle is approximately 10 deg. This tip speed is undesirable from a power standpoint, but does not appear to have control or flapping problems.

The orientation of the tip path plane, shown in Fig. 14, is another indication of the state of the rotor. It is the sum of the hub angle of attack and the longitudinal flapping. It only varies over a few degrees for the three tip speeds, but the contours bear some similarity to the contours of lift in Fig. 11. Where the lift increases in Fig. 11, the tip path plane angle increases. The absence of steep gradients indicates that the rotor orientation changes slowly with changes in collective pitch and airspeed.

Finally, rotor power, calculated as rotor drag multiplied by velocity, is shown in Fig. 15. The contributions to drag and power for this rotor are discussed in detail in Ref. 7. For the present study, the only interest is sharp gradients, especially with horizontal contours that indicate rapid changes with collective pitch. In Fig. 15, there are none. The rotor power is nearly independent of collective pitch, so from a power standpoint, any collective pitch setting is appropriate.

This is consistent with findings for a single collective pitch setting in Ref. 7 that power was dominated by profile power and interference and induced power were minor in comparison. Because the lift is strongly dependent on collective pitch in Fig. 11, but the power is not, the induced power must be

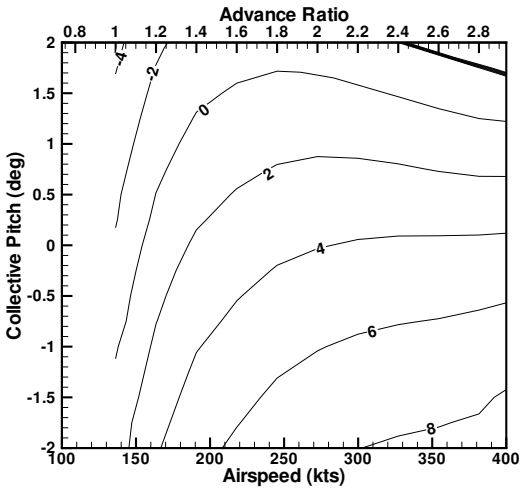

(a) V_T = 230 ft/sec

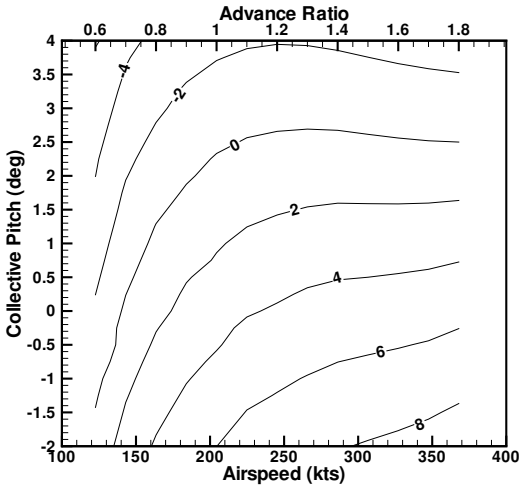

(b) V_T = 345 ft/sec

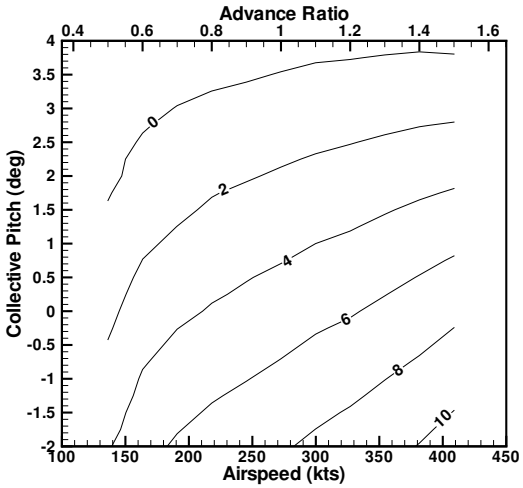

(c) V_T = 460 ft/sec

Fig. 12. Spindle tilt for a teetering rotor vs. airspeed and collective pitch, V_T = 230–460 ft/sec.

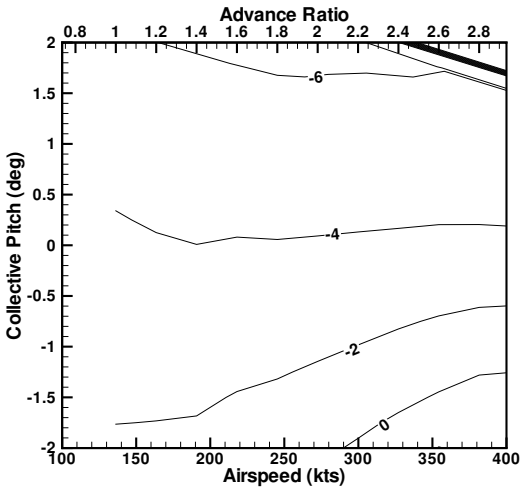

(a) V_T = 230 ft/sec

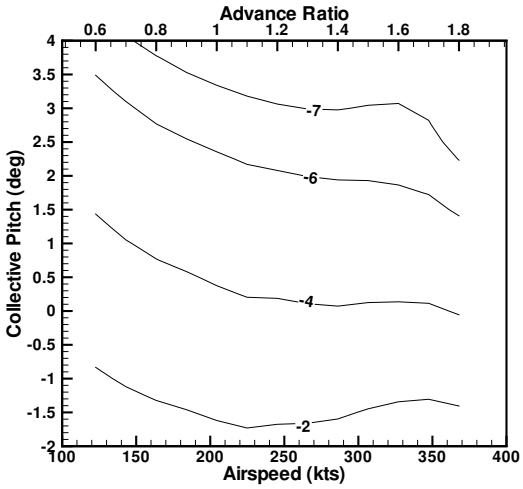

(b) V_T = 345 ft/sec

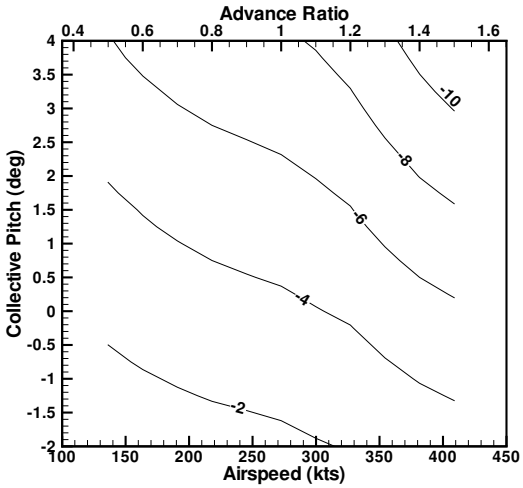

(c) V_T = 460 ft/sec

Fig. 13. Flapping angle for a teetering rotor vs. airspeed and collective pitch, V_T = 230–460 ft/sec.

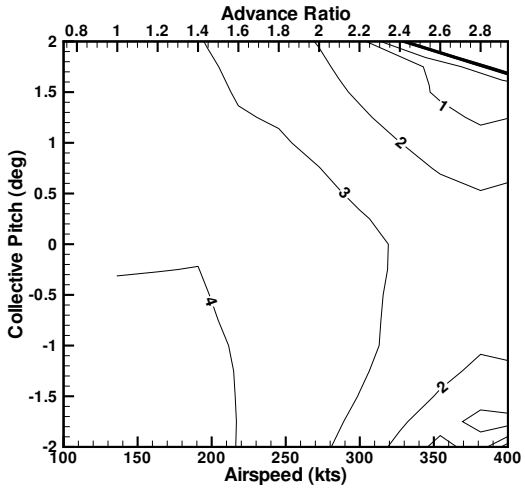

(a) V_T = 230 ft/sec

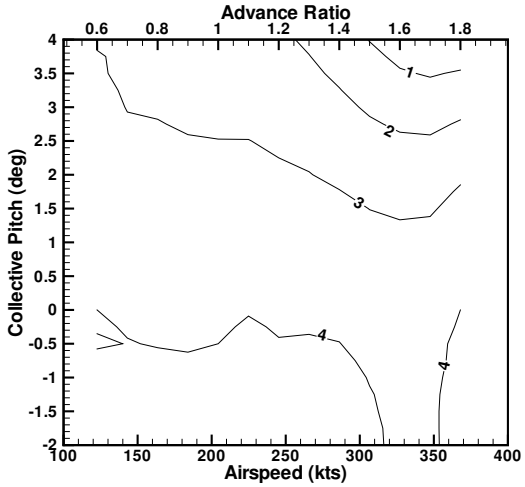

(b) V_T = 345 ft/sec

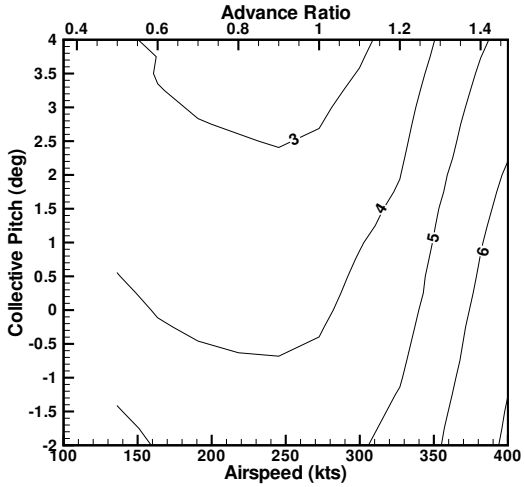

(c) V_T = 460 ft/sec

Fig. 14. Tip path plane angle of attack for a teetering rotor vs. airspeed and collective pitch, V_T = 230–460 ft/sec.

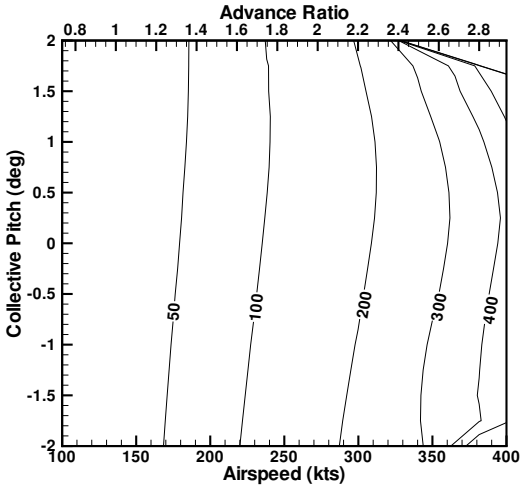

(a) V_T = 230 ft/sec

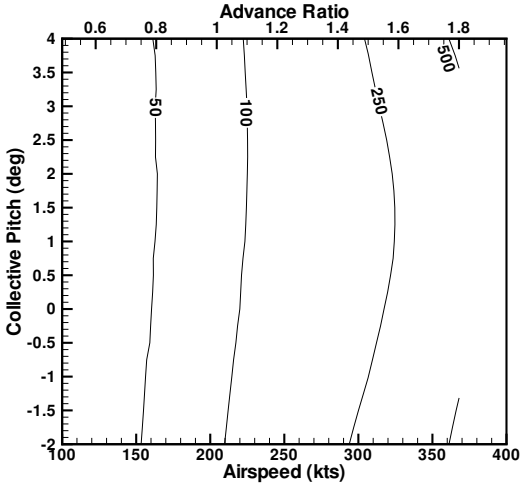

(b) V_T = 345 ft/sec

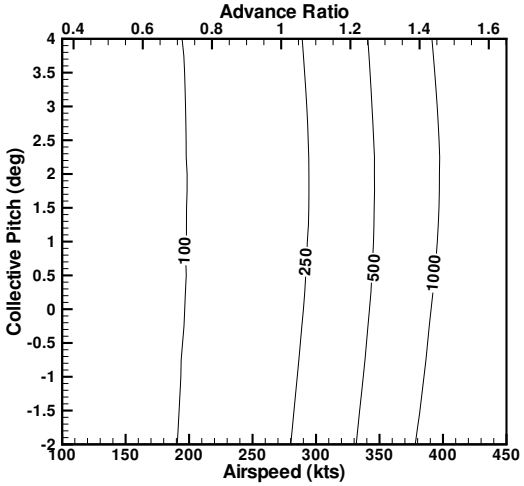

(c) V_T = 460 ft/sec

Fig. 15. Power required for a teetering rotor vs. airspeed and collective pitch, V_T = 230–460 ft/sec.

small relative to the profile power on the rotor. Given this, it is not a detriment for the rotor to carry lift.

These results provide guidance for an optimum collective pitch. The first clear conclusion is not to use the 460 ft/sec tip speed. The increased power required is clearly undesirable. For the lower tip speeds, the lift gradients do not translate into gradients in rotor power, so the optimum collective can be chosen based on control and flapping angles. These results, Figs. 12–13, oppose each other. Spindle tilt is minimized as collective pitch increases, but flapping is minimized for lower collective pitch. Therefore a moderate value in the 0–1 deg range is appropriate.

Articulated Rotor

The previous section described control calculations for a teetering rotor. The same results for an articulated rotor hinged at the center of rotation are shown in Figs. 16–20. The model used to calculate these results is the same as the teetering rotor except that the blades can now flap independently. The results for the 230 and 345 ft/sec cases are indeed very similar to those for the teetering rotor. The rotor lift, Fig. 16, increases at low collective pitch angles and high speed, and decreases to the point of being negative at high collective pitch angles and high speed. The 460 ft/sec articulated case is also quite similar to the 460 ft/sec teetering case.

The flapping, spindle tilt, and tip path plane angle are also similar to the teetering rotor. The flapping angle (Fig. 17) decreases with positive collective, and the spindle tilt (Fig. 18) decreases with negative collective. The change in slope of the contour lines between the 345 and 460 ft/sec tip speed cases is also present. The tip path plane angle tracks the rotor lift as well, and no steep gradients are present.

The power plots (Fig. 20) also look similar to those for the teetering rotor, except the power differences between the tip speeds are more pronounced. In Fig. 15, the differences between the 230 and 345 ft/sec tip speed cases were hardly noticeable. In Fig. 20, the differences are still not large but it is clear that the power is higher for the 345 ft/sec tip speed case. The power required for the 460 ft/sec tip speed case is significantly higher than that for the 345 ft/sec tip speed, again indicating that the rotor should not be operated at this speed.

The conclusion is that the optimum collective pitch should be in the middle of the collective range, although the power curves suggest that a bias toward lower collective pitch would reduce the power required by the rotor. Depending on the maximum speed for the vehicle, this would require a spindle tilt of 7–8 deg, which should be a tolerable control angle.

In summary, there do not appear to be any significant flying qualities or performance issues related to collective pitch. Depending on the tip speed and the design cruise speed, some benefit can be realized by careful selection of collective pitch,

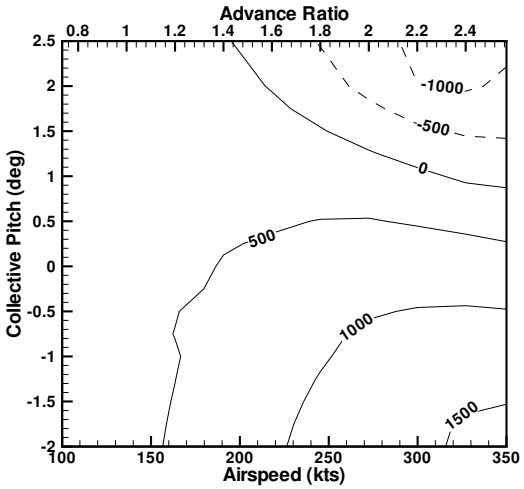

(a) V_T = 230 ft/sec

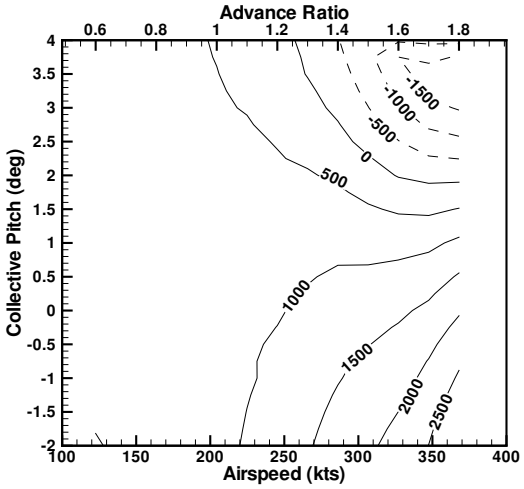

(b) V_T = 345 ft/sec

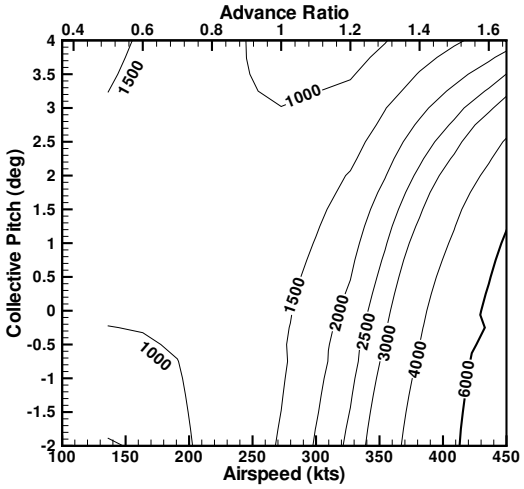

(c) V_T = 460 ft/sec

Fig. 16. Lift for an articulated rotor hinged at the center of rotation vs. airspeed and collective pitch, V_T = 230–460 ft/sec.

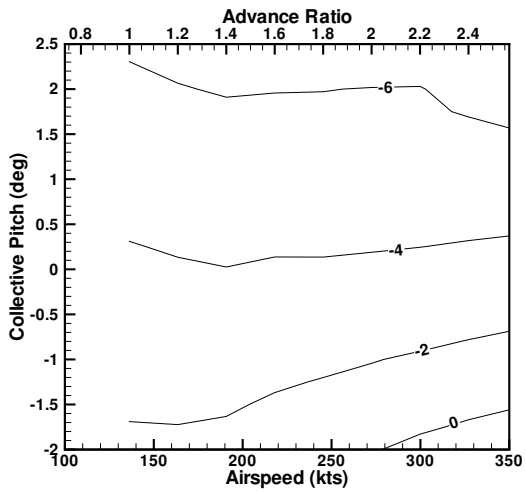

(a) V_T = 230 ft/sec

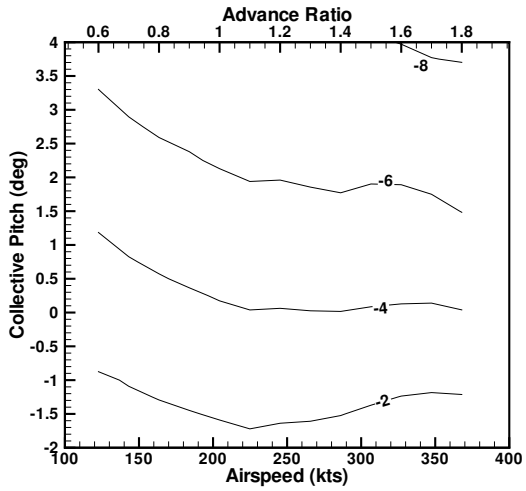

(b) V_T = 345 ft/sec

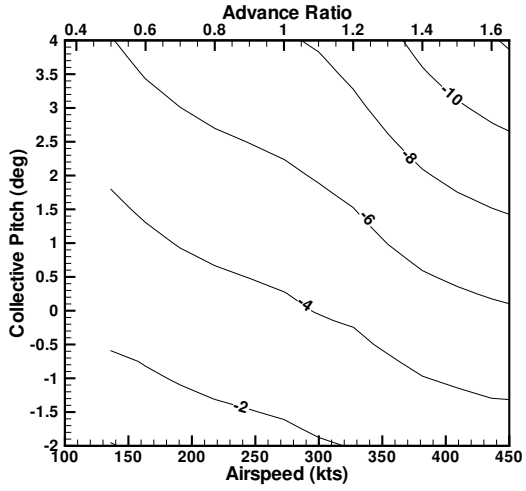

(c) V_T = 460 ft/sec

Fig. 17. Flapping angle for an articulated rotor hinged at the center of rotation vs. airspeed and collective pitch, V_T = 230–460 ft/sec.

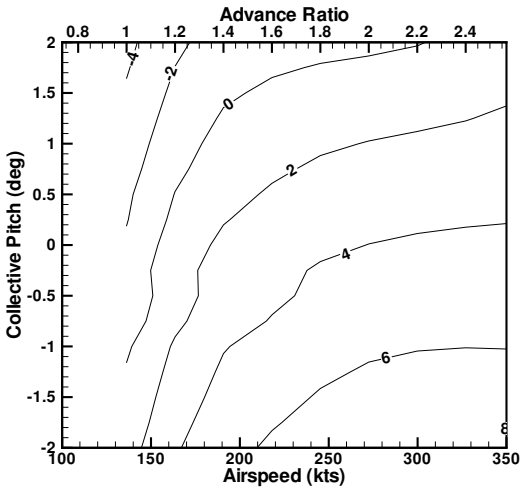

(a) V_T = 230 ft/sec

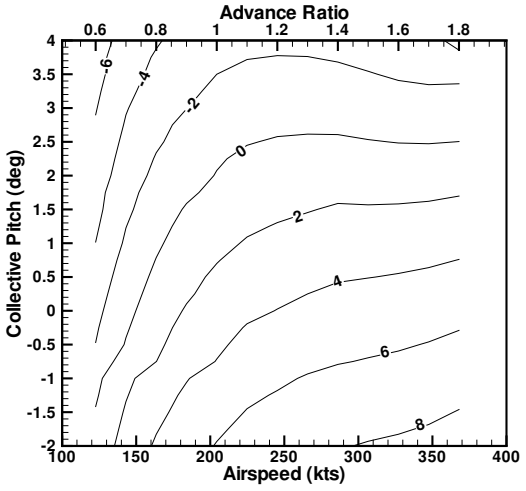

(b) V_T = 345 ft/sec

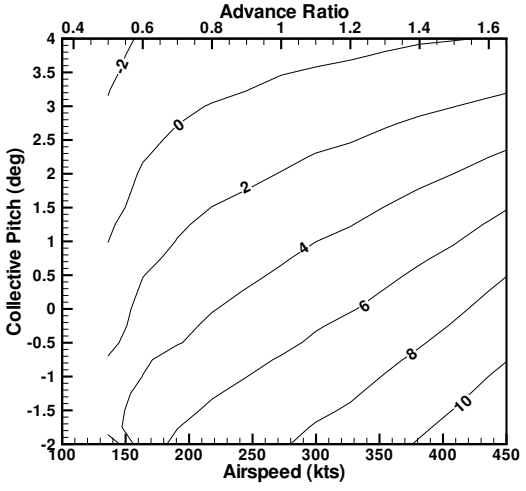

(c) V_T = 460 ft/sec

Fig. 18. Spindle tilt angle for an articulated rotor hinged at the center of rotation vs. airspeed and collective pitch, V_T = 230–460 ft/sec.

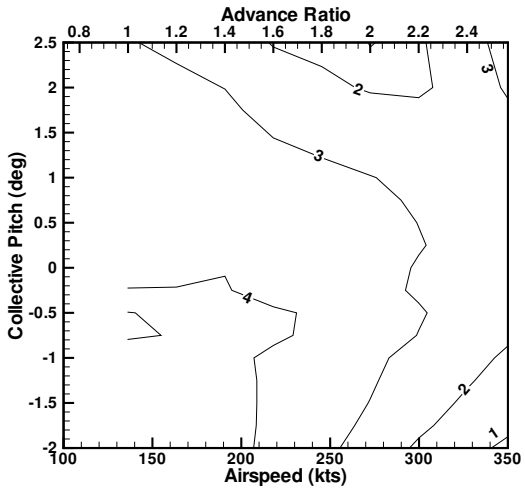

(a) V_T = 230 ft/sec

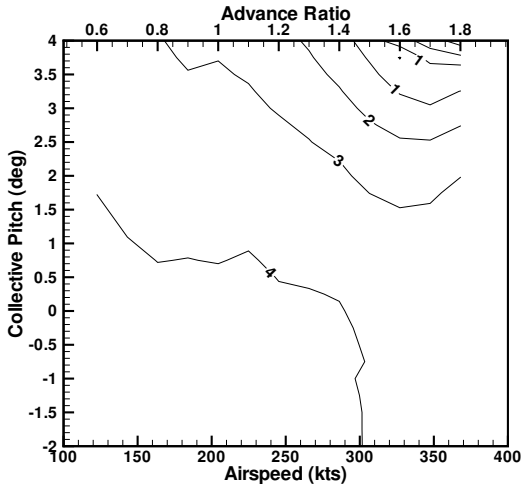

(b) V_T = 345 ft/sec

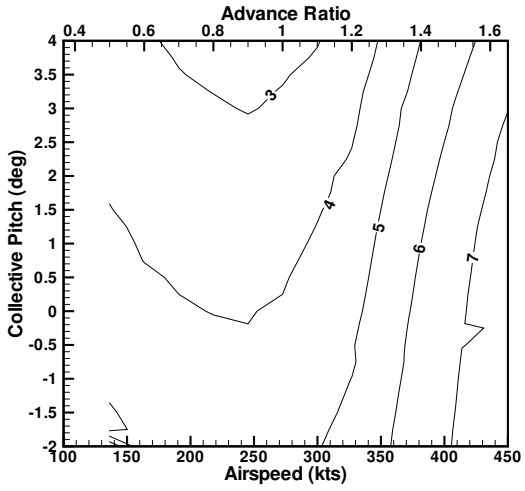

(c) V_T = 460 ft/sec

Fig. 19. Tip path plane angle of attack for an articulated rotor hinged at the center of rotation vs. airspeed and collective pitch, V_T = 230–460 ft/sec.

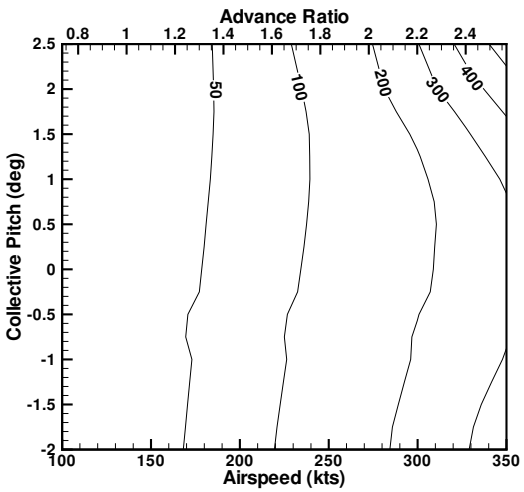

(a) V_T = 230 ft/sec

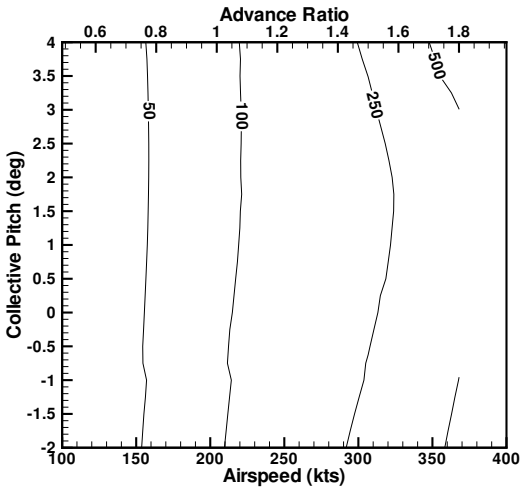

(b) V_T = 345 ft/sec

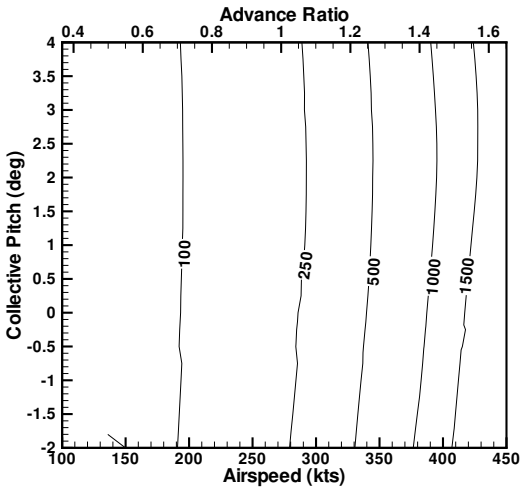

(c) V_T = 460 ft/sec

Fig. 20. Power required for an articulated rotor hinged at the center of rotation vs. airspeed and collective pitch, V_T = 230–460 ft/sec.

but adequate performance and controllability is possible over a range of collective pitch settings.

Elastic Blades

A generic CAMRAD II elastic blade model was developed to determine what effect elasticity has on stability. Structural dynamic properties for a production blade are preferable, but elastic properties for a high advance ratio rotor were not available. Instead, elastic properties were chosen to approximate what a production blade might have.

The model was intended to be as simple as possible. The blade has no chordwise offsets of center of gravity, tension center, or shear center, and uniform stiffness. The blade frequencies were designed based on a hover tip speed of 650 ft/sec. The flap and lag stiffness values were adjusted for a fundamental lag frequency near 1.2/rev and ratio of lag to flap stiffness of 30:1. Three separate torsion stiffness values were selected for comparison. They were chosen to produce fundamental torsion frequencies of 4.5/rev, 6.5/rev, and 8.5/rev at a 650 ft/sec tip speed.

A fan plot for the elastic blade model is shown in Fig. 21. The operating speeds and the speed at which the frequencies were set are shown by solid lines at 230, 345, 460, and 650 ft/sec. The solid symbols are flap and lag modes for the 4.5/rev torsion frequency. The flap and lag modes for the 6.5/rev and 8.5/rev torsion frequencies were nearly the same to the resolution of the plot, so they were not duplicated. The one exception is some interaction between the 4.5/rev torsion mode and the first elastic flap mode which is not present for the other two torsion frequencies. The modes for the three torsion frequencies are plotted on the same graph with open symbols, but it is important to realize that only one of the torsion modes is present in each model. Since the torsion frequencies are less dependent on RPM, the per rev frequencies at the operating speeds of 230–460 ft/sec are higher than 4.5/rev, 6.5/rev and 8.5/rev.

The stability of the elastic blades is shown in Figs. 22–24. Four modes were used in the elastic blade analysis, one each of teeter, elastic flap, lag, and torsion. The rigid blade teetering mode damping (the only degree of freedom for the rigid blade model) is also shown on the plots for comparison. For these results, the models were trimmed to zero power by tilting the shaft. The lowest tip speed of 230 ft/sec was chosen to eliminate the effects of compressibility. Once the trim condition was satisfied, Floquet theory was used to calculate system eigenvalues. The modes were identified by matching the frequency and damping to form continuous curves. The damping level shown is the real part of the eigenvalue, so negative numbers are stable, positive numbers unstable.

A hard stability boundary is evident near an advance ratio of 1.5 in Figs. 22–24. Although it appears from the plots that different modes become unstable, but at this boundary several

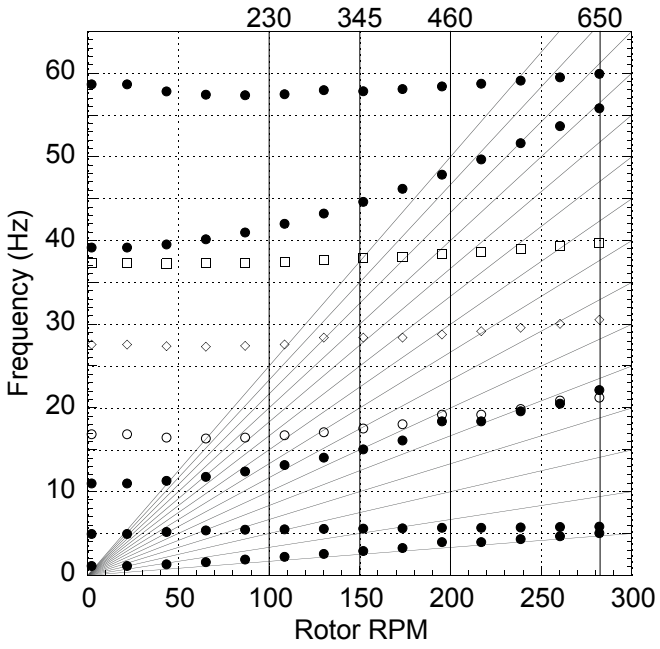

Fig. 21. Frequencies of the CAMRAD II elastic blade models with 4.5–6.5/rev torsion frequencies.

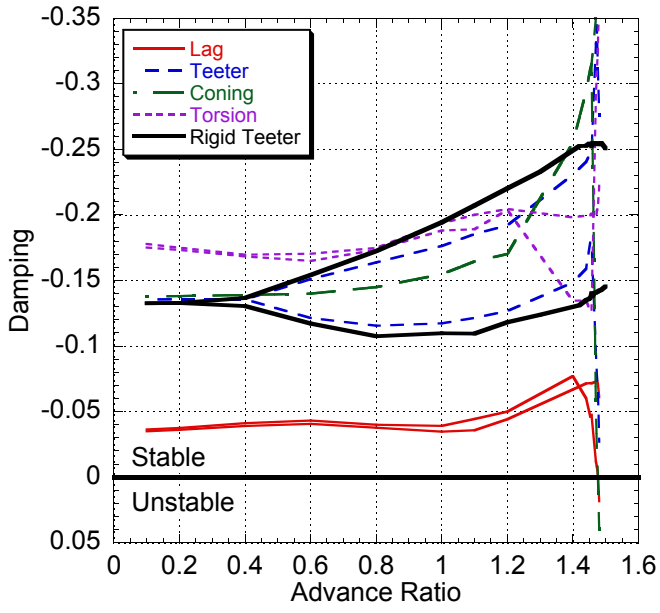

Fig. 22. Stability of elastic teetering rotor at tip speed V_T = 230 ft/sec and torsion frequencies of 4.5/rev.

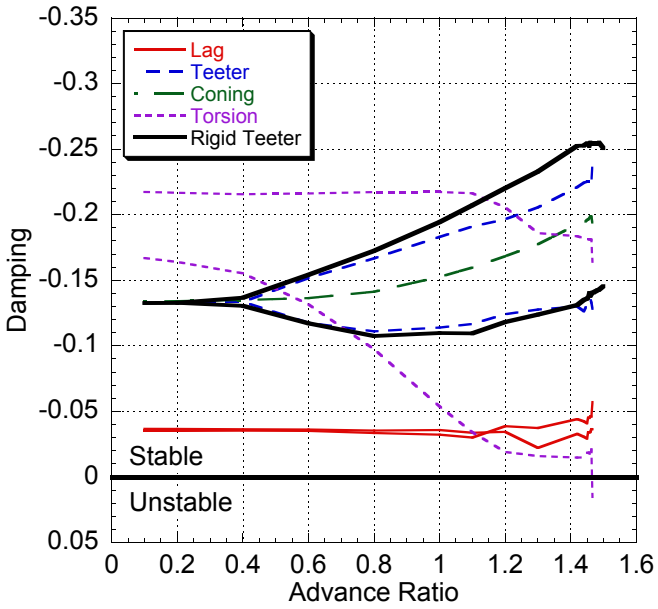

Fig. 23. Stability of elastic teetering rotor at tip speed V_T = 230 ft/sec and torsion frequencies of 6.5/rev.

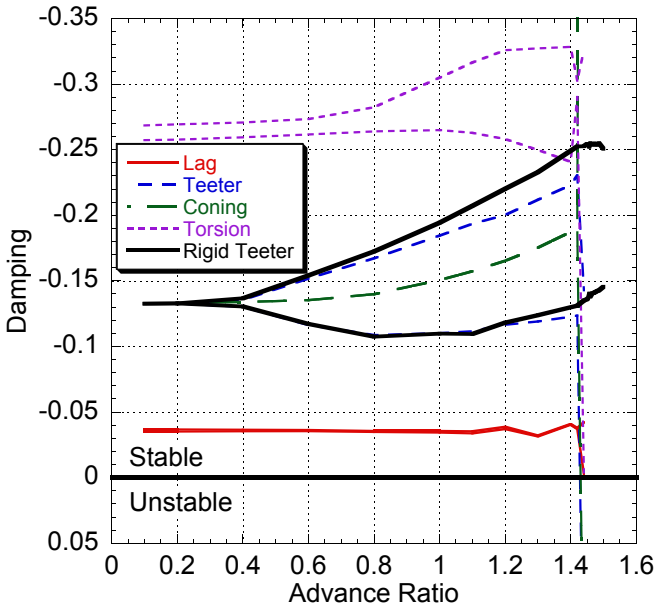

Fig. 24. Stability of elastic teetering rotor at tip speed V_T = 230 ft/sec and torsion frequencies of 8.5/rev.

modes become unstable at once. The modes become unstable very rapidly, so it is difficult to obtain a periodic solution and the damping levels (both stable and unstable) in this region are very sensitive to small changes in the trim state. Regardless of the damping levels, it is clear that the rigid blade shows no sign of instability while the elastic blades are clearly unstable and the stability boundary does not depend on the torsion frequency.

The elastic stability is very different from the rigid blade stability in Figs. 8 and 9. For the rigid blade, the rotor is stable to an advance ratio of 3, but for the elastic blade, there is a sharp stability boundary at an advance ratio of about 1.5. This reinforces the importance of elastic blade properties and shows that even for a teetering rotor, if the blades are not sufficiently stiff, an instability will occur.

The rotor thrust and power for these rotor models are shown in Figs. 25 and 26. These show that although there is a large difference in stability, there is almost no difference in performance. In Fig. 25, the lift for the 4.5/rev torsion frequency appears to deviate significantly from the other frequencies and the rigid blade. The approximately 200 lb of difference in lift represents only about 5% of the vehicle gross weight, so the deviation is actually small. When the torsion frequency is raised to 6.5/rev, the lift is nearly converged to the rigid blade result. The rotor power is dominated by profile power, so this deviation is almost imperceptible in Fig. 26. These results suggest that stability boundary is not caused by changes in the trim state resulting from elastic deflections, but is very sensitive to elastic stiffness.

Conclusions

The stability and control of rotors at high advance ratio applicable to a slowed-rotor compound helicopter have been investigated. A simple linear model, rigid blade CAMRAD II models, and an elastic blade CAMRAD II model were developed. The following conclusions are made:

1. The simplified flapping blade analysis suggested that a teetering rotor was the most stable hub configuration. The articulated rotor was unstable above an advance ratio of about 2.2 but could be stabilized to higher speed with δ_3. The gimbaled rotor was unstable above advance ratios of about 2 and was not stabilized by δ_3.

2. Damping predicted by the simplified analysis and a rigid blade CAMRAD II model were similar outside regions of rotor stall. Trimming the CAMRAD II model to an autorotation condition did not influence the stability.

3. Autorotation can be maintained at two distinct shaft angles for the same collective pitch setting. There is a sizeable difference in lift between the two trim conditions.

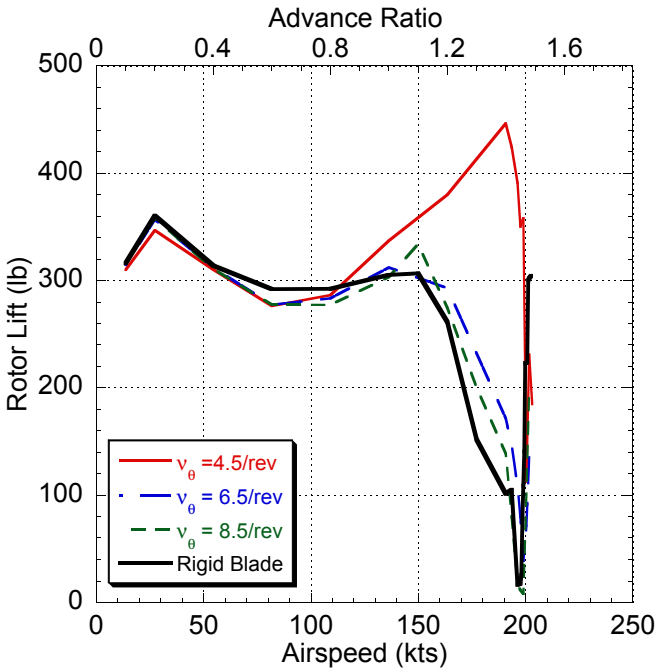

Fig. 25. Comparison of rotor lift for elastic and rigid blade teetering rotors, V_T = 230 ft/sec and elastic torsion frequencies of 6.5–8.5/rev and rigid.

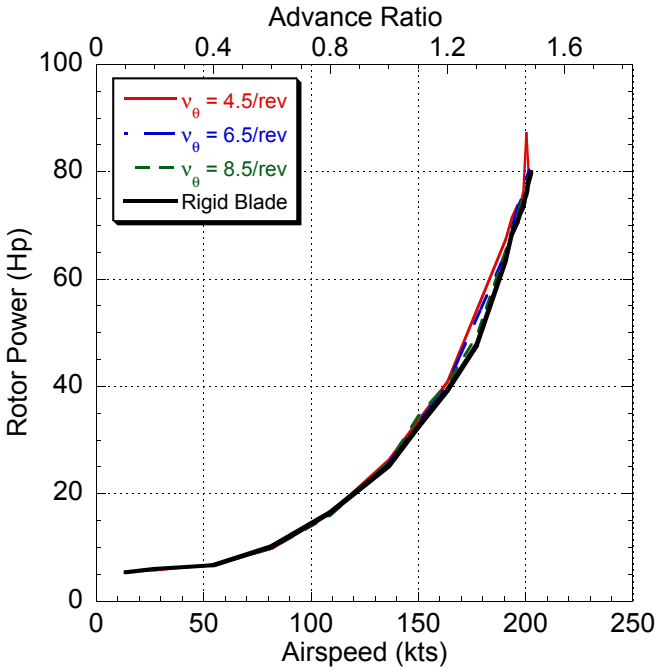

Fig. 26. Comparison of rotor power for elastic and rigid blade teetering rotors, V_T = 230 ft/sec and elastic torsion frequencies of 6.5–8.5/rev and rigid.

4. The optimum collective pitch for the four hub configurations—teetering, articulated with 0% and 5% hinge offset, and rigid—was found to be around 0–1 deg to minimize control input and flapping. There was no collective pitch restriction on power for the collective pitch ranges considered.

5. Rotor power required was only increased slightly by increasing the tip speed from 230 to 345 ft/sec, but a large increase was seen increasing from 345 to 460 ft/sec.

6. Blade elasticity was found to drastically reduce the rotor stability. For the particular blade stiffnesses considered, a sharp boundary was predicted near an advance ratio of 1.5. The blade elasticity did not significantly affect the rotor performance.

References

[1]Hohenemser, K., "A Type of Lifting Rotor with Inherent Stability," *Journal of the Aeronautical Sciences*, Vol. 17, September 1950.

[2]Hohenemser, K., "Remarks on the Unloaded Rotor Type of Convertiplane," Proceedings of the American Helicopter Society 11th Annual Forum, Washington, DC, April 1955.

[3]Hohenemser, K. H., "Some Aerodynamic and Dynamic Problems of the Compound Rotary-Fixed Wing Aircraft," Proceedings of the American Helicopter Society 8th Annual Forum, Washington, DC, May 1952.

[4]Hohenemser, K. H., "Aerodynamic Aspects of the Unloaded Rotor Convertible Helicopter," *Journal of the American Helicopter Society*, Vol. 2, (1), January 1957.

[5]Hickey, D. H., "Full-Scale Wind-Tunnel Tests of the Longitudinal Stability and Control Characteristics of the XV-1 Convertiplane in the Autorotating Flight Range," NACA RM A55K21a, Ames Aeronautical Laboratory, May 1956.

[6]Marks, M. D., "Flight Test Development of the XV-1 Convertiplane," *Journal of the American Helicopter Society*, Vol. 2, (1), January 1957.

[7]Floros, M. W. and Johnson, W., "Performance Analysis of the Slowed-Rotor Compound Helicopter Configuration," Proceedings of the American Helicopter Society 4th Decennial Specialists' Conference on Aeromechanics, San Francisco, CA, January 2004.

[8]Sissingh, G. J., "Dynamics of Rotors Operating at High Advance Ratios," *Journal of the American Helicopter Society*, Vol. 13, (3), July 1968.

[9]Peters, D. A. and Hohenemser, K. H., "Application of Floquet Transition Matrix to Problems of Lifting Rotor Stability," *Journal of the American Helicopter Society*, Vol. 16, (2), April 1971.

[10]Carter Jr., J., “CarterCopter—A High Technology Gyroplane,” Proceedings of the American Helicopter Society Vertical Lift Aircraft Design Conference, San Francisco, CA, January 2000.

[11]Johnson, W., “Rotorcraft Aeromechanics Applications of a Comprehensive Analysis,” Heli Japan 98: AHS International Meeting on Advanced Rotorcraft Technology and Disaster Relief, Nagarafukumitsu, Gifu, Japan, April 1998.

[12]Floros, M. W. and Johnson, W., “Stability Analysis of the Slowed-Rotor Compound Helicopter Configuration,” Proceedings of the American Helicopter Society 60th Annual Forum, Baltimore, MD, June 2004.